

# Thin-film rupture for large slip

D. Peschka · A. Münch · B. Niethammer

Received: 14 July 2008 / Accepted: 28 September 2009 / Published online: 22 October 2009  
© Springer Science+Business Media B.V. 2009

**Abstract** The rupture of thin liquid films on hydrophobic substrates, assuming large slip at the liquid-solid interface, is studied using a recently developed *strong slip* lubrication model, it is shown that the rupture passes through up to three self-similar regimes with different dominant balances and different scaling exponents. For one of these regimes the similarity is of second kind, and the similarity exponent is determined by solving a boundary-value problem for a nonlinear ODE. Furthermore, finite-time rupture is proved for this regime.

**Keywords** Asymptotic behavior of solutions · Jet break-up · Lubrication theory · Self-similarity · Self-similar solutions of second kind

## 1 Introduction

The formation of singularities is a well-studied topic in the context of viscous liquids when describing the evolution towards rupture of thin films or towards pinch-off of a liquid thread [1–6]; see also the reviews (and many references therein) by Oron et al. [7] and by Eggers [8]. Eggers also wrote some of the pioneering papers in the field of jet break-up and droplet formations, e.g. [9]. The study of these processes has a variety of technological applications in drying, spin coating and in the semiconductor technology where nanoscopic thin films are deposited, furthermore in jet spraying, to name a few. Understanding the relevant forces and their influence on the rupture process will be important for the application to be successful. Fundamental driving forces that have been considered in the past include van der Waals forces, surface tension, inertia, and viscous forces.

Ida and Miksis [4] consider rupture of a free film in a regime where viscous forces and van der Waals forces dominate the rupture process. They, find that the evolution has a self-similar phase, where the scaling exponents can not be determined from dominant balances alone. They, however, do not explain how the exponents which they determine from numerical simulations of the PDE are fixed; this was later done for a related problem of curvature-driven jet break-up by Papageorgiou [10].

---

D. Peschka  
Weierstraß Institute for Applied Analysis and Stochastics (WIAS), Mohrenstraße 39, 10117 Berlin, Germany

A. Münch (✉) · B. Niethammer  
Mathematical Institute, University of Oxford, 24-29 St. Giles', Oxford OX1 3LB, UK  
e-mail: muench@maths.ox.ac.uk

Based on earlier work on the break-up of jets by Brenner et al. [11], Vaynblat et al. [6] investigate the same model as Ida and Miksis but in a regime where viscous forces, inertia and van der Waals forces balance. This dominant balance leads to similarity solutions of the first kind. In their ODE analysis they find an intricate family of self-similar profiles, from which the time-dependent film dynamics selects the one of “lowest order”. In [12, 13] Bernoff and Witelski study the self-similar structure of rupture of a thin film on a solid substrate with a fourth-order thin-film model that incorporates surface tension, van der Waals interaction, viscosity and a no-slip condition at the liquid–solid interface. Again they find a family of self-similar profiles where only one is stable and is selected from the dynamics of the time-dependent PDE model.

A fundamental property of all these models is that the singularity occurs in finite time, i.e., the spatial minimum of the film thickness tends to zero as a singularity time  $t_* < \infty$  is approached. Surprisingly enough, there has been very few rigorous analytical work regarding this phenomenon. A notable exception is a short but inspiring paper by Renardy [14] on the finite-time singularity for a model for curvature-driven jet pinch-off that includes viscosity (but not inertia or longitudinal surface tension) as the dominant forces.

In recent applications, where liquid polymer films of nanoscale thickness are deposited on hydrophobized substrates, rupture of the film is a ubiquitous phenomenon that initiates the dewetting of the liquid. The onset of rupture as well as later stages of dewetting and the morphology and dynamics that arise in the course of the film evolution have been intensively studied both experimentally and theoretically. Experiments show intricate patterns arising at the beginning of rupture and also in the hole and residual droplet distribution, e.g. [15, 16]. For many of these processes, it has been found that effective interfacial slippage (which usually plays a minor role in most classical thin-film problems, being mostly considered near moving contact-lines to alleviate the stress singularity) significantly influences the dynamics and the morphology of the evolving film structures [17–19].

For these situations, new lubrication models have been developed [20–22] for rupture and post-rupture processes. The models by Münch et al. [21] have been used to explain the spanwise instability at the rim around the widening hole [23] as well as the morphology of the cross-section of the rim [19]. Recently, the models have been studied with respect to slow dynamics of the droplets into which the liquid has collected in the late phases of the dewetting process [24]. This research comes at a time of rising interest in slip at liquid–solid boundary conditions in a broader range of applications; see the recent review by Lauga et al. [25].

In this paper, we investigate the dynamics of the rupture process of a dewetting film on a solid substrate when slip is very large. This work connects with the previous research in that this previous research considered limiting situations with either very small/zero slip or very large/infinite slippage. Therefore, studying these models relates to these other applications.

The outline of the paper is as follows. In Sect. 2, we briefly summarize the thin-film models for dewetting films with various degrees of slippage. Through asymptotic considerations and balancing arguments, as well as numerical simulations, we identify in Sect. 3 three different scaling regimes for the self-similar phases of the rupture for the models with large slip. One of these regimes turns out to be of second kind, and for this regime we analyze the similarity ODE and determine the similarity exponent. This regime lends itself to a rigorous analysis with respect to finite-time blow-up, which we prove in Sect. 4. Conclusions and outlook on future work are given in Sect. 5.

## 2 Formulation

The problem of a viscous, incompressible layer of fluid in the domain

$$\Omega_T = \{(X, Z) \in \mathbb{R}^2 : 0 \leq Z \leq H(X, T), -L \leq X \leq L\}$$

with the free boundary  $\{Z = H(X, T)\}$  is modeled by the Navier–Stokes equations

$$\rho(U_T + UU_X + WU_Z) = \mu \nabla^2 U - (P + F)_X,$$

$$\rho(W_T + WW_X + WW_Z) = \mu \nabla^2 W - P_Z,$$

$$U_X + W_Z = 0.$$

The potential energy  $F = AH^{-3}$  ( $A > 0$ , Hamaker constant) describes the attractive van der Waals interaction between the free boundary and the solid–liquid interface at  $\{Z = 0\}$ .

These equations in the bulk are supplemented by the kinematic condition and a tangential and normal-stress balance at the free boundary, which are

$$\begin{aligned} H_T - W + UH_X &= 0, \\ (U_Z + W_X)(1 - H_X^2) + 2H_X(W_Z - U_X) &= 0, \\ P - 2\mu \frac{(1 - H_X^2)W_Z - H_X(U_Z + W_X)}{1 + H_X^2} + \sigma \frac{H_{XX}}{(1 + H_X^2)^{3/2}} &= 0, \end{aligned}$$

respectively. At the solid–liquid interface we assume impermeability and a Navier-slip condition

$$W = 0 \quad \text{and} \quad U = BU_Z,$$

whereas at the artificial boundary  $\{X = \pm L\}$  we prescribe a contact angle  $\pi/2$  and impose a no-flux condition

$$H_X|_{\pm L} = 0 \quad \text{and} \quad U|_{\pm L} = 0.$$

We introduce a scale for each variable,

$$\begin{aligned} Z &= \tilde{H}z, \quad H = \tilde{H}h, \quad B = \tilde{H}b, \quad X = \tilde{L}x, \quad L = \tilde{L}l, \\ U &= \tilde{U}u, \quad W = \tilde{W}w, \quad T = \tilde{T}t, \quad P + F = \tilde{P}p, \quad F = \tilde{P}\phi. \end{aligned}$$

The scale  $\tilde{H}$  represents the typical film thickness, whereas  $\tilde{L}$  is a scale for the typical length. For our particular choice of scales the van der Waals pressure, which drives the film rupture, and the pressure from surface tension, which tends to counteract it, are simultaneously present. Balancing pressure with the van der Waals and the surface term, respectively, yields

$$\tilde{L} = \left(\frac{\sigma}{A}\right)^{1/2} \tilde{H}^2, \quad \text{and} \quad P = \sigma \frac{\tilde{H}}{\tilde{L}^2}.$$

The velocity scales arise from balancing  $U_{ZZ}$  with the pressure gradient and by balancing the two terms in the continuity equation; the time scale is set by the kinematic condition

$$\tilde{U} = \frac{\tilde{P}\tilde{H}^2}{\mu\tilde{L}}, \quad \tilde{W} = \frac{\tilde{H}}{\tilde{L}}\tilde{U}, \quad \text{and} \quad \tilde{T} = \frac{\tilde{L}}{\tilde{U}}. \quad (2.1)$$

For thin-film theory to be applicable, the ratio of height scale to length scale must be small, i.e.,

$$\epsilon = \frac{H}{L} = \frac{(A/\sigma)^{1/2}}{\tilde{H}} \ll 1;$$

under this condition, we can expand the Navier–Stokes equations in terms of the small parameter  $\epsilon$ . It was shown in [21] that, depending on the relative magnitude of the two other parameters, namely, the Reynolds number and the scaled slip, which are, respectively,

$$\text{Re}_* = \frac{\rho\sigma\tilde{H}}{\mu^2} \quad \text{and} \quad b = \frac{B}{\tilde{H}},$$

not one but a whole family of leading-order models arise.

If we generally assume that  $\text{Re}_*$  is  $O(1)$ , there are two distinguished limits for  $\epsilon \rightarrow 0$ : The weak-slip model,

$$h_t = - \left[ \left( \frac{1}{3}h^3 + bh^2 \right) (h_{xx} - h^{-3}) \right]_x, \quad (2.2)$$

is obtained for moderate slip length, i.e.,

if  $b$  is held fixed at  $O(1)$  as  $\epsilon \rightarrow 0$ . For

$$b = \nu/\epsilon^2, \quad \text{where} \quad \nu = O(1),$$

fixed, the choice of velocity and time scales (2.1) is not consistent with the limit  $\epsilon \rightarrow 0$ . Rather, the proper choice results from balancing the pressure and  $W_{ZZ}$  term in the second component of the Navier–Stokes equations, that is,

$$\tilde{U} = \frac{\tilde{P}\tilde{L}}{\mu}, \quad \tilde{W} = \frac{\tilde{H}}{\tilde{L}}\tilde{U} \quad \text{and} \quad \tilde{T} = \frac{\tilde{L}}{\tilde{U}}. \quad (2.3)$$

Then,  $\epsilon \rightarrow 0$  results in the strong-slip model,

$$h_t + (hu)_x = 0, \quad (2.4a)$$

$$\text{Re}_*(u_t + uu_x) = \frac{4}{h}(hu_x)_x + (h_{xx} - h^{-3})_x - \frac{u}{\nu h}, \quad (2.4b)$$

which describes the dynamics of the film profile and average flow velocity for large (strong) slippage.

The models that we derived for other relative magnitudes of  $b$  can be obtained as limits of these two models. If  $b$  is small, we get the no-slip lubrication equation that is simply (2.2) with  $b$  set to zero. In the scaling regime with  $1 \ll b \ll \epsilon^{-2}$  and appropriate velocity and time scales, we get the intermediate slip model

$$h_t = - \left[ h^2 (h_{xx} - h^{-3}) \right]_{x \downarrow x}, \quad (2.5)$$

which arises in the limit  $\nu \rightarrow 0$  from the strong-slip model (after rescaling time and velocity appropriately) or  $\tilde{b} \rightarrow \infty$  from the weak-slip model (after rescaling time with  $b$ ). Finally, in the model for very large slip, i.e.,  $\epsilon^{-2} \ll b$  or equivalently  $1 \ll \nu$ , the last term in (2.4b) drops out:

$$h_t + (hu)_x = 0,$$

$$\text{Re}_*(u_t + uu_x) = \frac{4}{h}(hu_x)_x + (h_{xx} - h^{-3})_x.$$

This “free slip” model describes freely suspended films, i.e., the slip length is infinite. They are discussed by Vaynblat et al. [26] with respect to their similarity structure.

In this paper we will be mostly concerned with the slip lengths that lie in the strong-slip regime, including the limiting situation of intermediate slip, and assume that we are considering very viscous liquids where  $\text{Re}_* \ll 1$ .

### 3 Phases of rupture

#### 3.1 Onset of rupture

We consider here the situation where rupture is initiated by a small perturbation of the flat state  $h \equiv 1, u \equiv 0$ . Letting

$$h(x, t) = 1 + \delta h_0 \exp(ikx + \lambda t) \quad \text{and} \quad u(x, t) = \delta u_0 \exp(ikx + \lambda t)$$

in (2.4) one obtains to  $O(\delta)$  the eigenvalue problem

$$iku_0 + \lambda h_0 = 0,$$

$$-4k^2 u_0 - ik^3 h_0 + 3ikh_0 - \nu^{-1} u_0 - \text{Re}_* \lambda u_0 = 0,$$

which has the two solutions

$$\lambda_{\pm}(k) = \frac{1}{2\nu \text{Re}_*} \left( -1 - 4\nu k^2 \pm \sqrt{(1 + 4\nu k^2)^2 - 4 \text{Re}_* \nu^2 k^2 (k^2 - 3)} \right).$$

The eigenmode that corresponds to the minus sign is always stable, while the other eigenmode is unstable if  $0 < k^2 < 3$ .

For  $\nu \rightarrow 0$  and  $\text{Re}_* \ll \nu^{-2}$ , i.e., in particular for small and moderate Reynolds number  $\text{Re}_*$ , the dominant growth rate is given by

$$\frac{\lambda_+(k)}{\nu} = 3k^2 - k^4. \quad (3.1)$$

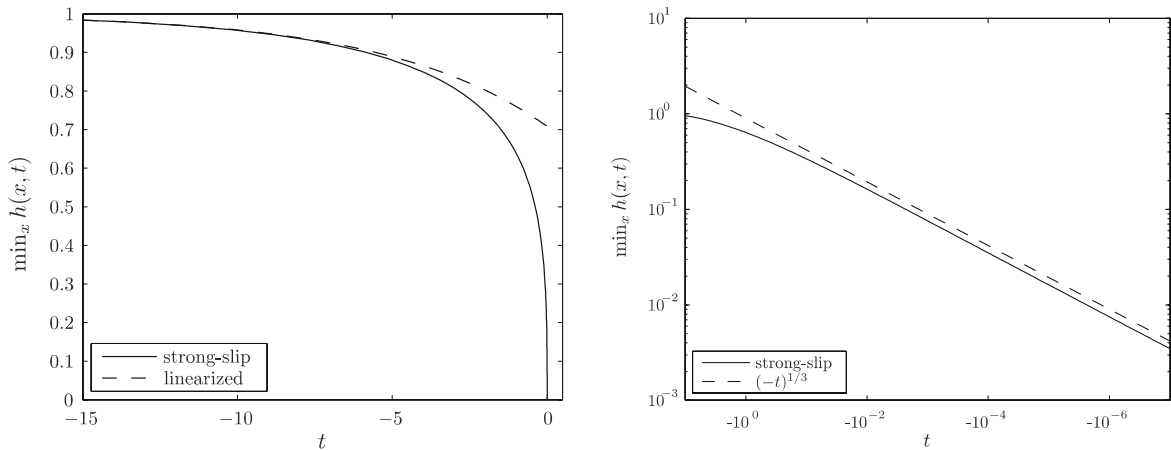


**Fig. 1** The evolution of  $\min_x h(x, t)$  for  $b = \text{Re}_* = 1$  compared to linearization has  $(-t)^{1/3}$  behavior as it quickly approaches zero at  $t = t_* = 0$

Except for a rescaling in time, this is exactly the eigenmode resulting from a linear stability analysis for the intermediate slip model (2.5) and is therefore the adequate model for the early evolution of the perturbation. Note that the wavenumber  $k_m$  for which the growth rate is maximal is  $k_m = \sqrt{3/2}$ . The typical growth of a perturbation with an eigenmode compared to a solution of the fully nonlinear model can be seen in Fig. 1.

### 3.2 Similarity analysis for the nonlinear evolution

As the perturbation grows, nonlinear terms in the model become important so that at later stages, we solve the model equations (2.4) numerically using a finite-difference scheme using adaptive time-stepping and a non-uniform grid that is regularly remeshed to concentrate points near where the film thickness is minimal. Boundary conditions were  $h_x = 0$  and  $u = 0$  at  $x = 0, l$ .

Unless stated otherwise, we set  $\text{Re}_* = 10^{-5}$ ,  $\nu = 10^{-8}$  and use the initial data  $h(x, 0) = 1 + 0.2 \cos(\pi x/4)$  and  $u(x, 0) = 0$  on the finite interval  $0 < x < l$  with  $l = 8$ . We impose the boundary conditions

$$h_x(x, 0) = 0, \quad h_x(x, l) = 0, \quad u(x, 0) = 0, \quad u(x, l) = 0.$$

The numerical solution in Fig. 2 shows that the decay of the global minimum of  $h$ ,  $h_{\min} = \min_x h(x, t) = h(x_*, t)$  with  $x_* = 4$  initially follows the prediction from the linear stability but then accelerates and tends to zero as  $t$  approaches a finite time  $t_*$ .

Moreover, appropriate rescalings of  $x$ ,  $h$  and  $u$  in time suggests that the solutions follow a self-similar behavior in a neighborhood of  $x_*$  as  $t \rightarrow t_*$ . We therefore make the ansatz

$$h(x, t) = (t_* - t)^\alpha H(\eta), \quad u(x, t) = (t_* - t)^\gamma U(\eta), \quad (3.2)$$

where  $\eta = (x - x_*)/(t_* - t)^\beta$  and with  $\alpha > 0$ ,  $\beta > 0$ . Note that the variables  $H$  and  $U$  are distinct from those used in Sect. 2. The restrictions on  $\alpha$  and  $\beta$  ensure that  $h$  and the lateral length scale shrink as  $\tau \rightarrow 0$ .

Upon inserting (3.2) into (2.4), it becomes immediately apparent that this system of equations does not permit an exact self-similar scaling, so it is necessary to identify which terms determine the evolution near rupture.

we consider as before the case when  $\nu \ll 1$  and  $\text{Re}_* \ll 1$ . It turns out that rupture passes through three different similarity regimes. All three regimes balance the terms in the mass conservation equations (2.4a), which, upon inserting (3.2), enforces  $\gamma = \beta - 1$ .

In view of the linear-stability results we expect that the first self-similar regime is governed by the terms that appear in the intermediate slip model, i.e., that surface tension and the finite-slip term enter the dominant balance

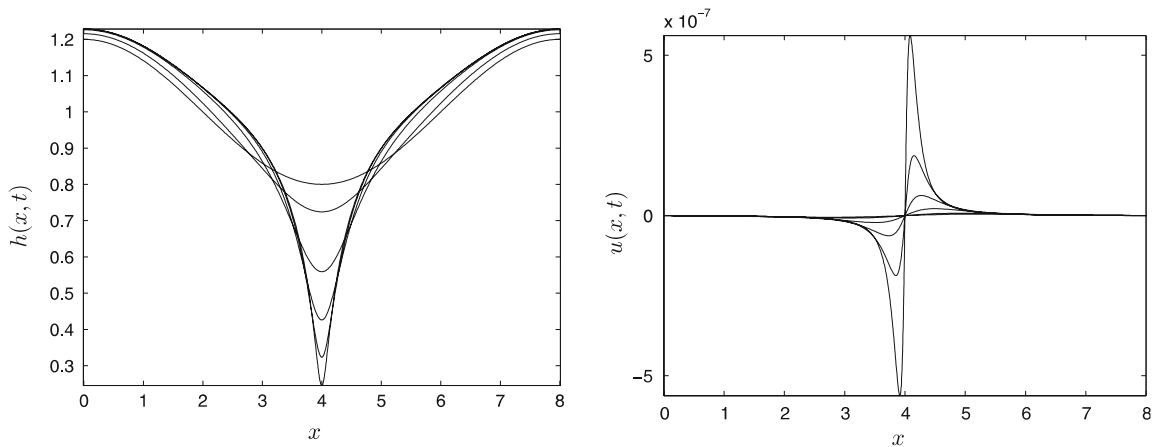


**Fig. 2** Solutions  $h(x, t)$  and  $u(x, t)$  during the early stage of rupture

at least initially if  $\nu$  is small and  $\text{Re}_*$  is not too large. Setting the exponents of the  $\tau$ -powers for these two terms to zero entails  $\alpha = 1/6$ ,  $\beta = 1/3$  and thus  $\gamma = -2/3$ . The remaining powers of  $t_* - t$  then have exponents  $-5/6$  for the inertial terms and  $-1/2$  for the Trouton term. Therefore, this similarity regime, which we label regime I, cannot persist indefinitely but the time period where it is valid can be increased if  $\nu$  and  $\text{Re}_*$  are decreased. A similar self-similar regime was studied by Witelski and Bernoff [12]. Using the no-slip condition at the liquid–solid interface they find  $\alpha = 1/5$  and  $\beta = 2/5$ .

If  $\text{Re}_*$  is sufficiently small, the Trouton term will be the first to enter the dominant balance; after that, we achieve a new self-similar state which includes this new term.

Inserting (3.2) into (2.4) using  $\gamma = \beta - 1$  yields

$$\alpha H - \beta \eta H' - (HU)' = 0, \quad (3.3a)$$

$$\text{Re}_* \tau^{3\alpha+2\beta-2} (\beta \eta U' - (\beta - 1)U + UU') = 4\tau^{3\alpha-1} \frac{(HU)'}{H} + \tau^{4\alpha-2\beta} H''' + 3 \frac{H'}{H^4} - \tau^{2\alpha+2\beta-1} \frac{U}{\nu H} \quad (3.3b)$$

If  $\text{Re}_*$  is sufficiently small, inertia does not enter the dominant balance in this regime. Furthermore if the Trouton term has to be in the dominant balance for this second self-similar regime, we must have  $\alpha = 1/3$ . Another balance is needed to fix  $\beta$ , but it is unclear at this stage which (if any) is the appropriate balance, so we treat  $\beta = \beta_{II}$  as a yet unknown parameter. We can, however, place some bounds on  $\beta_{II}$ ; to ensure that the exponents for the surface tension and finite-slip term are non-negative, we must require  $1/6 \leq \beta_{II} \leq 2/3$ . Qualitatively similar behavior has been studied in [10] and by Brenner et al. [11], but so far was not studied for thin-film rupture.

If  $\beta_{II} < 1/2$ , the exponent of the  $\tau$ -power for the inertial terms is negative and this term will become of order one when  $\tau \sim \text{Re}_*^{1/(1-2\beta)}$ . This suggests a third self-similar regime, regime III, where inertia enters the dominant balance, thus  $3\alpha + 2\beta - 2 = 0$ . Including the finite-slip term in the dominant balance yields  $\beta < 0$ , which violates the local nature of rupture in (3.2), and including surface tension would yield a negative exponent for the  $\tau$  coefficient for the Trouton term, which is also inconsistent. Thus, the only consistent choice is to balance inertia and the Trouton term,  $3\alpha - 1 = 0$ , therefore,  $\alpha = 1/3$  and  $\beta = 1/2$ . Self-similar solutions for this balance have been found and studied in some detail by Vaynblat et al. [6] and by Ida and Miksis [4].

Summarizing, we expect to see up to three self-similar regimes if  $\nu \ll 1$  and  $\text{Re}_*$  small enough. In all regimes we have  $\gamma = \beta - 1$ , whereas the other two exponents are  $\alpha = 1/6$  and  $\beta = 1/3$  in regime I,  $\alpha = 1/3$  and  $\beta = \beta_{II}$  in regime II, and  $\alpha = 1/3$  and  $\beta = 1/2$  in regime III. Note that  $\beta_{II}$  is not yet determined. The three regimes are traversed in order  $I \rightarrow II \rightarrow III$ , if  $\beta_{II} < 1/2$  and  $\text{Re}_*$  is small enough.

We now investigate our numerical results more closely to verify the above considerations and also to determine what happens with  $\beta = \beta_{II}$  in the second regime.

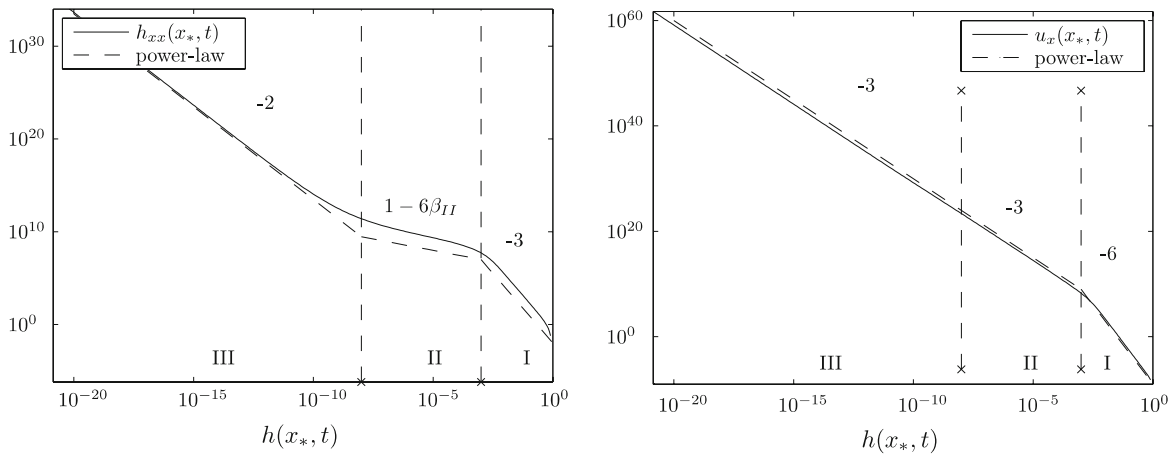


**Fig. 3** Solution of the strong-slip equation with  $\text{Re}_* = 10^{-5}$ ,  $b = 10^{-8}$  has distinct regions I, II, III where  $u_x(x_*, t)$  and  $h_{xx}(x_*, t)$  evolve like a power of  $(t_* - t)$ ; the predicted power is indicated by the *dashed* line with the exponent written above

Figure 3 shows a double-log plot of  $h_{xx}(x_*, t)$  and  $u_x(x_*, t)$  versus  $h(x_*, t)$ . In time regimes where the solution evolves self-similarly according to (3.2), the graph for  $h_{xx}(x_*, t)$  and  $u_x(x_*, t)$  will be straight lines with slope  $(\alpha - 2\beta)/\alpha$  and  $-1/\alpha$ , respectively. We can clearly distinguish three different regimes where both lines are straight, connected by two relatively sharp transitions connecting these lines. This clearly suggests that we have three different self-similar regimes.

We now compare these slopes with our predictions for each of the three regimes, and, in the case of regime II, extract the missing value for  $\beta_{II}$ . In regimes I and III, we expect the slopes to be  $(\alpha - 2\beta)/\alpha = -3$ ,  $-1/\alpha = -6$  and  $(\alpha - 2\beta)/\alpha = -2$ ,  $-1/\alpha = -3$ . Dashed auxiliary piecewise straight lines that have these slopes in each regime are shown in Fig. 3 close to the corresponding graphs and good agreement of the slopes can be seen.

In regime II, we know that the line for  $u_x(x_*, t)$  must have a slope  $-1/\alpha = -3$  and the auxiliary line with this slope is indeed parallel to the graph for  $u_x(x_*, t)$ . From the other line, we can determine the slope by a linear fit. To obtain higher accuracy, we carried out another numerical simulation with  $\text{Re}_* = 0$  which eliminates the third regime and then continued the calculation to very small values of  $h_{\min} = h(x_*, t)$ . The linear fit with the line  $h_{xx}(x_*, t)$  resulted in the value  $\beta_{II} = 0.248930 \pm 3 \times 10^{-6}$ .

This value differs markedly from  $1/6$  or  $2/3$  for which either the finite-slip or the surface-tension term would enter the balance of the dominant terms, respectively. For the value of  $\beta_{II}$  found, these terms are subdominant, leaving no possibility for another balance. The self-similar behavior in this regime is therefore an example for a self-similar solution of the second kind [27, Chap. 3]. For these solutions, the missing exponent cannot be found from a simple application of balancing of terms or conservation law, but by actually solving the similarity ODE system where  $\beta = \beta_{II}$  enters as an unknown.

### 3.3 Second kind similarity solution

We start with the system (2.4) and drop all terms that we have found to be subdominant in our previous considerations; specifically, in (2.4b), we only retain the Trouton viscosity and the van der Waals term. Then we introduce the self-similar ansatz (3.2) with  $\alpha = 1/3$  and  $\gamma = \beta - 1$  but keeping  $\beta = \beta_{II}$  as an unknown parameter. After integrating and rearranging the equations, we obtain the following second-order ODE system

$$U_\eta = \frac{3}{8H^3} + \frac{C}{H}, \quad (3.4a)$$

$$H_\eta = \frac{H}{U + \beta\eta} \left( \frac{1}{3} - \left[ \frac{3}{8H^3} + \frac{C}{H} \right] \right), \quad (3.4b)$$

where  $C$  is an arbitrary constant of integration. The self-similar solution is an inner solution that describes the evolution near  $x_*$  as  $t$  approaches the rupture time, i.e. for small  $\tau$ . Matching to the outer solution requires

$$\lim_{\eta \rightarrow \pm\infty} U(\eta) = 0. \tag{3.5}$$

From this we can conclude that the denominator in (3.4b) must be zero for some  $\eta = \eta_0$ . For  $H$  to be analytic there, the term in parentheses must be zero, which implies

$$C = \frac{H(\eta_0)}{3} - \frac{3}{8H(\eta_0)^2}$$

and  $U_\eta(\eta_0) = 1/3$ . This also implies that  $\eta_0$  is unique, i.e.,  $U + \beta\eta$  is zero only for this value of  $\eta = \eta_0$ . If we focus only on solutions for which  $H$  is symmetric (and  $U$  anti-symmetric), we must have  $\eta_0 = 0$ . If we introduce  $H_0 = H(0)$ , we can formulate the problem of finding the self-similar solution at this stage as follows: solve (3.4) with

$$C = \frac{H_0}{3} - \frac{3}{8H_0^2} \tag{3.6}$$

and initial conditions

$$U(0) = \frac{1}{3}, \quad H(0) = H_0, \tag{3.7}$$

and find  $H_0$  and  $\beta$  such that (3.5) is satisfied for  $\eta \rightarrow \infty$ . This imposes only one condition for two free parameters, and indeed upon solving the ODE system numerically it turns out that for each  $H_0$  we can find exactly one  $\beta = \beta_1(H_0)$  for which the solution of (3.4) and (3.7) satisfies (3.5). We note that  $\beta_1$  is a monotonic increasing function of  $H_0$ .

A second condition arises from the requirement that  $U$  and  $H$  are analytic at  $\eta = 0$ , i.e.,  $U$  and  $H$  can be written as Taylor series

$$U(\eta) = \sum_{n=0}^{\infty} U_n \eta^{n+1}, \quad H(\eta) = \sum_{n=0}^{\infty} H_n \eta^n.$$

Due to symmetry, all terms with odd  $n$  must vanish in both series. Inserting this ansatz into (3.4) yields the recursion relation

$$\begin{pmatrix} H_0^3(k+1) & H_0^2 - 2CH_0 \\ 0 & H_0^2(\beta + \frac{1}{3})k - H_0^2 + 2CH_0 \end{pmatrix} \begin{pmatrix} U_k \\ H_k \end{pmatrix} = \begin{pmatrix} \alpha_k \\ \beta_k \end{pmatrix}, \tag{3.8}$$

where  $\alpha_k$  and  $\beta_k$  are homogeneous functions of the previous coefficients  $U_n, H_n$  with  $n < k$ . Specifically,  $\alpha_2 = 0$  and  $\beta_2 = 0$ . If the matrix on the left-hand side of (3.8) is non-singular for all  $k$ , this implies that all coefficients of the Taylor expansions must vanish for  $n > 1$  leading to trivial solutions. Therefore, the determinant of the matrix must vanish for at least one  $k = n \geq 2$ , which implies that

$$\beta = \beta_2(H_0; n) \equiv \frac{9 - 4H_0^3(n-1)}{12H_0^3n} \tag{3.9}$$

for this  $n$ . Upon choosing an even  $n$ , this provides the second condition on  $\beta$  and  $H_0$ . The function  $\beta_2$  of  $H_0$  is monotonic decreasing, thus for each even  $n$  there is exactly one pair of  $\beta$  and  $H_0$  for which the solution of (3.4) and (3.7) satisfies both (3.5) and (3.9). Numerically obtained values for  $\beta$  and  $H_0$  for the first three values of  $n$  are shown in Table 1.

We note that  $\beta$  seems to be monotonic decreasing with increasing  $n$  and that for  $n \leq 4$  the values of  $\beta < 1/6$ . This would lead to an inconsistency, i.e., the finite-slip term in (3.3b) would have a coefficient with a negative power of  $\tau$ . For  $n = 2$ , the resulting value for  $\beta$  is in excellent agreement with the value for  $\beta_{II}$  extracted from the numerical solution of the PDE near rupture.

The difference to the formal approach for similarity solutions of first kind, as for example in [6,26], is that the approach for second kind self-similar solutions contains an additional parameter  $\beta$ . This parameter is fixed by requiring the recursion matrix for the formal power-expansion to be singular, as it is done in [10,11].



**Table 1** Solutions for higher  $n$  with corresponding  $\beta$  and  $H_0$  values

$n$	$\beta$	$H_0$
2	0.2489306	0.9663168
4	0.1280401	0.7915672
6	0.0877860	0.6992785

## 4 Finite-time singularity formation

### 4.1 Lagrangian formulation

In regime II, where viscosity dominates, inertia is negligible, and the slip parameter is infinite, the evolution is described by the PDE

$$h_t + (hu)_y = 0, \quad (4.1a)$$

$$\frac{4}{h}(hu_y)_y - \left(h^{-3}\right)_y = 0. \quad (4.1b)$$

The singularity occurs already after a finite time, i.e., there exists a finite time  $t_*$ , such that the quantity

$$\frac{1}{\min h(y, t)}$$

is unbounded as the time  $t$  approaches  $t_*$ .

As it was done by Renardy [14], we now pass over to a Lagrangian formulation<sup>1</sup> for (4.1). To this end, we introduce the transformation  $\phi(\cdot, t) : [0, 1] \rightarrow [0, 1]$  via

$$\phi_t(x, t) = u(\phi(x, t), t),$$

$$\phi(x, 0) = \phi_0(x),$$

where  $\phi_0 : [0, 1] \rightarrow [0, 1]$  is a continuously differentiable monotonic mapping of  $[0, 1]$  onto itself; we will make a more specific choice later on. In particular we have  $y = \phi(x, t)$ . The spatial derivative  $s(x, t) \equiv \phi_x(x, t)$  satisfies

$$s_t(x, t) = u_x(\phi(x, t), t) s(x, t),$$

$$s(x, 0) = \phi_{0,x}(x),$$

from which we conclude that  $s(x, t) > 0$  for all  $x \in [0, 1]$  and  $t \geq 0$ . This in turn implies that  $\phi(\cdot, t) : [0, 1] \rightarrow [0, 1]$  is a monotonic mapping. Moreover, the boundary conditions imposed on  $u(0, t)$  and  $u(1, t)$  and the fact that  $\phi_0(0) = 0$ ,  $\phi_0(1) = 1$  imply that it is a one-on-one mapping of  $[0, 1]$  onto itself, for all  $t \geq 0$ , from which we also deduce that

$$\int_0^1 s(x, t) dx = 1 \quad \text{for } t \geq 0. \quad (4.2)$$

Letting  $\bar{h}(x, t) \equiv h(\phi(x, t), t)$  and  $\bar{u}(x, t) \equiv u(\phi(x, t), t)$ , application of the chain rule and (4.1) and integration shows that  $\bar{h}$  and  $\bar{u}$  satisfy

$$\bar{h}(x, t) s(x, t) = c(x), \quad (4.3)$$

$$\frac{s_t(x, t)}{s(x, t)} = \frac{3}{8} \left( \frac{1}{\bar{h}(x, t)^3} - \frac{C(t)}{\bar{h}(x, t)} \right), \quad (4.4)$$

<sup>1</sup> From now on  $x$  is a Lagrangian coordinate; previously it was the Eulerian one.

where  $c(x)$  and  $C(t)$  arise as constants of integration that do not depend on  $t$  or  $x$ , respectively. We can use (4.3) to eliminate  $\bar{h}$  from (4.4). For this purpose, it is useful to choose  $\phi_0$  as

$$\phi_0(x) = \int_0^x \frac{C_1}{\bar{h}(\xi, 0)} d\xi \quad \text{with } C_1 = \left[ \int_0^1 \frac{C_1}{\bar{h}(\xi, 0)} d\xi \right]^{-1}. \quad (4.5)$$

Then,

$$s(x, 0) = \phi_{0,x}(x) = \frac{C_1}{\bar{h}(x, 0)} \quad (4.6)$$

and therefore  $c(x) = C_1$  is independent of  $x$ , so that

$$s(x, t) = \frac{C_1}{\bar{h}(x, t)}. \quad (4.7)$$

Using this to eliminate  $\bar{h}$  from (4.4), we get

$$s_t(x, t) = s(x, t)^2 \left( s(x, t)^2 - C_1 C(t) \right).$$

Integrating this equation with respect to  $x$  from  $x = 0$  to  $x = 1$  and using (4.2) finally yields

$$s_t(x, t) = s(x, t)^2 \left( s(x, t)^2 - s_0^2(t) \right), \quad (4.8a)$$

where

$$s_0^2(t) = \int_{\Omega} s(x, t)^4 dx \Big/ \int_{\Omega} s(x, t)^2 dx, \quad (4.8b)$$

where we have introduced  $\Omega \equiv [0, 1]$ . In addition, we need to supply initial data  $s(0, x) = s_i(x)$  for  $x \in \Omega$ . Since  $s(0, x)$  is obtained from the initial data for  $\bar{h}$  via (4.6), we may assume that  $s_i(x)$  is non-negative, bounded and normalized in the sense

$$\int_{\Omega} s_i(x) dx = 1. \quad (4.9)$$

Let  $s_{\max}(t) \equiv \max_x s(x, t)$ . Since the evolution defined by (4.8) is locally Lipschitz, unique solutions exist by virtue of the Picard–Lindelöf theorem and can be extended as long  $s_{\max}(t)$  remains finite.

In view of (4.7), a blow-up of  $s$  is equivalent to  $\min_x \bar{h}(x, t) \rightarrow 0$ , i.e. pinch-off of the film. We will therefore focus on the question if and when  $s_{\max}(t)$  grows unboundedly and if so, if and when the blow-up occurs in finite time.

## 4.2 Examples and properties

Blow-up of  $s$  does not occur for all initial data. In the following example we show that one can easily construct stationary solutions; these solutions are in particular bounded. For example consider the following class of solutions of (4.8)

$$s(x, t) = \begin{cases} \frac{1}{\delta} & \text{in } \omega \subset \Omega \\ 0 & \text{elsewhere,} \end{cases} \quad (4.10)$$

where the size of the set  $\omega$  such that is  $|\omega| = \delta > 0$ . Solutions with positive initial data that can be decomposed:

$$s_i(x) = \begin{cases} s_{\max}(0) & \text{in } \omega \subset \Omega \\ s_i(x) < s_{\max}(0) & \text{elsewhere} \end{cases} \quad (4.11)$$

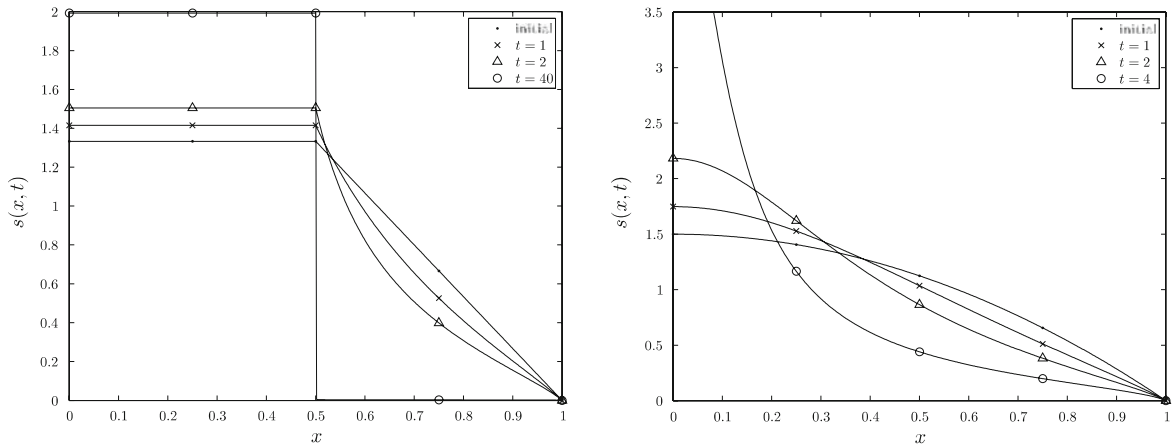


**Fig. 4** Numerical solutions of (4.8) with  $s_i(x) = \min\{4/3, 8/3(1-x)\}$  (solution is bounded  $s(x, t) < 2$ ) and  $s_i = 3/2(1-x^2)$  (solution is unbounded) for different times, respectively

along with property (4.9) and  $|\omega| > 0$  are bounded in time and converge to these stationary solutions. Note that this initial data is not necessarily continuous in  $x$ , and the problem formulation (4.8) does not really require it to be continuous, though in physically motivated situations we may choose to restrict our considerations to this case or even smoother initial data.

In Fig. 4 we show two numerical solutions of (4.8). The solution which is shown in the left panel of Fig. 4 is bounded,  $s(x, t) < 2$ , and seems to converge to

$$s(x, t) \rightarrow \begin{cases} 2 & x \in [0, 1/2] \\ 0 & x \in (1/2, 1] \end{cases}$$

as  $t$  goes to infinity. The solution shown in the right panel of Fig. 4 diverges increasingly fast until the numerical scheme is unable to resolve the singularity of  $s(x, t)$  at  $x = 0$ . Later we will analyze this type of singular solutions quantitatively.

Examining properties of (4.8) will be helpful to prove blow-up of  $s$  later. The properties proven here are generic for this type of integro-differential equation and do not depend too much on the special form of the equation. Some rather simple observations are that (4.8) conserves the property

$$\int_{\Omega} s(x, t) dx \equiv 1 \quad \forall t \in [0, t_*),$$

that  $s_0 = 1$  if and only if  $s = 1$  almost everywhere in  $\Omega$ , and that  $\partial_t s_{\max} \geq \partial_t s$ .

**Lemma 4.1** (Properties of solutions) *Solutions of the integro-differential equation (4.8) and the related functions  $s_{\max}(t)$  and  $s_0(t)$  obey the following properties:*

1. Estimate from above and below:

$$s_{\max}(t) \geq s_0(t) \geq 1. \quad (4.12a)$$

2. Monotonicity of  $s_{\max}$  and  $s_0$ :

$$\partial_t s_{\max}(t) \geq 0 \quad \text{and} \quad \partial_t s_0(t) \geq 0. \quad (4.12b)$$

3. For continuous solutions  $s_{\max}(t) > s_0(t) > 1$  if and only if the set

$$M_{\epsilon}(t) = \{x \in \Omega : \epsilon < s(x, t) < s_0(t) - \epsilon\}$$

has strictly positive measure for some  $\epsilon > 0$ .

*Proof 1.* The first inequality follows from  $\int s^4 dx \leq s_{\max}^2 \int s^2 dx$ , while the second is shown using Cauchy–Schwarz inequalities

$$s_0^2 = \frac{\int s^4 dx}{\int s^2 dx} \geq \int s^2 dx \geq \left( \int s dx \right)^2 = 1. \quad (4.13)$$

2. The first part is trivial. For the second part consider  $\partial_t(s_0^2)$  explicitly

$$\begin{aligned} 2s_0\partial_t s_0 &= \frac{4 \int (\partial_t s) s^3 dx}{\int s^2 dx} - \frac{2 \int (\partial_t s) s dx \int s^4 dx}{\left( \int s^2 dx \right)^2} \\ &= \left( \int s^2 dx \right)^{-1} \left( 2s_0^4 \int s^3 dx - 6s_0^2 \int s^5 dx + 4 \int s^7 dx \right) \\ &\equiv \left( \int s^2 dx \right)^{-1} (A s_0^4 + B s_0^2 + C). \end{aligned}$$

This expression is non-negative, if  $s_0^2 \leq (-B - \sqrt{B^2 - 4AC}) / 2A$ . Using

$$B^2 - 4AC = 36 \left( \int s^5 dx \right)^2 - 32 \int s^3 dx \int s^7 dx \stackrel{\text{C.S.}}{\leq} 4 \left( \int s^5 dx \right)^2$$

one finds

$$s_0^2 \leq \left( \int s^5 dx \right) / \left( \int s^3 dx \right) \Leftrightarrow \partial_t s_0 \geq 0.$$

The assertion follows directly from Cauchy–Schwarz inequalities

$$\left( \int s^4 dx \right)^2 \leq \int s^5 dx \int s^3 dx$$

and

$$\left( \int s^3 dx \right)^2 \leq \int s^4 dx \int s^2 dx.$$

3. The implication  $s_0 > 1$  follows from the property, that  $s_0 = 1$  if and only if  $s = 1$  almost everywhere. Assume  $s_{\max} = s_0$ , then

$$0 = s_{\max}^2 - s_0^2 = \frac{\int s^2 (s_{\max}^2 - s^2) dx}{\int s^2 dx}$$

implies that  $s(x, t) \in \{0, s_{\max}\}$  almost everywhere, contrary to the assumption that  $M_\epsilon$  has a finite measure. On the other hand suppose  $M_\epsilon$  is empty for all  $\epsilon > 0$ , then  $s$  is either zero or  $s_0 \leq s \leq s_{\max}$ . Since the integrand in

$$0 = \int_{\Omega} s^2 (s^2 - s_0^2) dx = \int_{\Omega \setminus M_0} s^2 (s^2 - s_0^2) dx \geq 0,$$

is nonnegative, this expression can only be zero if  $s \in \{0, s_0\}$  almost everywhere, which implies  $s_{\max} = s_0$ .  $\square$

### 4.3 Unboundedness of solutions

Conservation of mass  $\int_0^1 s(x, t) dx = 1$ , non-negativity  $s(x, t) \geq 0$ , and uniqueness of solutions imply that solutions are bounded if the maximum is attained on a finite interval. Figure 4 showed a numerical example for such a behavior.

Before we proceed, we give a short motivation why it is not very restrictive to consider only decreasing initial data. This assumption is, however, very useful to make the forthcoming analysis much more concise.

*Remark* For given  $s \in C([0, 1]; \mathbb{R}^+)$  think of  $\bar{s} \in C([0, 1]; \mathbb{R}^+)$  being defined as follows: Let  $x_s(r) = \mu(y \in [0, 1] : s(y) \geq r)$  and let  $\bar{s}$  be the largest decreasing, function on  $[0, 1]$  with

$$\bar{s}(x_s(r)) = r. \quad (4.14)$$

This mapping retains some key properties of  $s$ , i.e.,  $\text{ess sup } s = \text{ess sup } \bar{s}$ ,  $s_0 = \bar{s}_0$ , which is even true for solutions of (4.8) with initial data  $s_i$  and  $\bar{s}_i$ . The solution map  $s \mapsto s(t, \cdot)$  and the ordering map (4.14)  $s \mapsto \bar{s}$  commute.

From now on we will only consider decreasing initial data; uniqueness of solution of (4.8) implies that  $s(x, t)$  is decreasing in  $x$  for all  $t$ . Therefore define the set

$$P(t) = [0, p(t)] = \{x \in \Omega : s(x, t) \geq s_0(t)\}$$

and  $N(t) = \Omega \setminus P(t) = (p(t), 1]$  the complement of  $P(t)$  in  $\Omega = [0, 1]$ .

In the following theorem it is shown that if the maximum of  $s_i$  is only attained in a single point, i.e. at zero, then  $s_{\max}(t)$  is unbounded.

**Theorem 4.2** (Unboundedness of solutions) *If the decreasing initial data of (4.8) obeys  $s_{\max}(0) > s_i(x)$  for  $x > 0$ , then  $s_{\max}(t)$  is unbounded in time.*

*Proof* Conversely assume that  $s$  is bounded for all times. Due to the monotonicity property (4.12b),  $s_0$  and  $s_{\max}$  converge and must have the same limits  $s_0, s_{\max} \rightarrow K < \infty$ . Using  $P(t)$  and  $N(t)$  volume conservation yields

$$1 = \int_{\Omega} s(x, t) dx \leq p(t) K + \int_{N(t)} s(x, t) dx. \quad (4.15)$$

Suppose  $p(t)$  is bounded from below by a positive  $\delta$ . For any  $0 < x \leq \delta < p(t)$  the definition of  $\partial_t s$  in (4.8) implies that  $s_{\max}(t) - s(x, t)$  increases in time and thus the inequality  $s_{\max}(t) - s_0(t) \geq s_{\max}(t) - s(\delta, t) \geq s_{\max}(0) - s_i(\delta) > 0$ , is a contradiction to convergence  $s_0, s_{\max} \rightarrow K$  showing that  $p(t)$  must converge to zero. One easily sees that  $s(x, t) \rightarrow 0$  for any fixed  $x \in N(t)$  as  $t \rightarrow \infty$  so that both terms on the right-hand side of (4.15) go to zero. This shows that the assumption is wrong and  $s_{\max}(t)$  must be unbounded.  $\square$

The time-dependent maximum  $s_{\max}(t)$  is unbounded, if the maximal value of  $s_i(x)$  is attained only in a single point. Unfortunately this proof does not produce any quantitative information about the speed of the blow-up of  $s$ . If more information about the initial data are available, in particular about the behavior near the maximum, one can compute an upper bound on the blow-up time and a lower bound for the blow-up rate explicitly. Suppose  $s_i(x)$  is bounded from above near the maximum at  $x = 0$  like

$$s_i(x) \leq s_{\max}(0) - f(x),$$

where  $f(x)$  is increasing with  $f(0) = 0$ . We will prove that  $s_{\max}(t)$  is unbounded for some finite time if there exists an upper bound with  $f(x) = Cx^n$  for some  $C, n > 0$ . The proof is quite explicit and reproduces the blow-up rates of the corresponding self-similar solution.

### 4.4 Finite-time blow-up

In the introduction we claimed that in many thin-film models rupture occurs after a finite time. We showed that this is the case for all numerical solution of the intertialess strong-slip equation. Now we prove that the corresponding

simplified integro–differential equation (4.8) has this feature as well and we will check whether the singularity develops at the same rate.

The strategy of our proof consists of two steps: First we consider a general bound  $s_i(x) \leq s_{\max}(0) - f(x)$  for the initial data and define a time evolution for  $f$  such that

$$s(x, t) \leq s_{\max}(t) - f(x, t).$$

For  $x \in P(t)$  we estimate  $f(x, t)$  from below.

Second, since  $P(t)$  is decreasing, we should find an efficient estimate on  $p(t)$  from below, i.e.  $0 < \tilde{p}(t) \leq p(t)$ . Then it holds that

$$s_{\max}(t) \geq s_{\max}(t) - s_0(t) \geq f(t, p(t)) \geq f(t, \tilde{p}(t)).$$

If one expresses  $\tilde{p}(t)$  in terms of  $s_{\max}(t)$  and  $t$  and integrates both sides of the inequality it turns out that the right-hand side diverges after a finite time. Hence  $s_{\max}(t)$  diverges after a finite time. For some parts of this proof we follow and generalize the ideas of Renardy [14].

The computation of a lower bound is quite simple; as before  $s(x, t)$  denotes the exact solution of problem (4.8) and  $s_0(t)$  is the functional defined in (4.8b). For any  $x$  with  $s_i(x) \leq s_{\max}(0) - f(x)$  define  $f(x, t) = s_{\max}(t) - \sigma(x, t)$ , where  $\sigma(x, t)$  is the solution of the ordinary differential equation

$$\sigma_t = \sigma^2 \left( \sigma^2 - s_0^2(t) \right). \tag{4.16}$$

with initial data  $s_{\max}(0) - f(x)$ . Uniqueness of solutions implies that  $f(x, t)$  defines an upper bound in terms of  $s(x, t) \leq s_{\max}(t) - f(x, t)$ . The following lemma gives an explicit lower bound for  $f(x, t)$ .

**Lemma 4.3** *For any  $x$  in a small neighborhood of  $x = 0$ , let  $\sigma$  be a solution of (4.16) with initial data  $\sigma(0) = s_{\max}(0) - f(x)$ . Let  $s(x, t)$  be decreasing in  $x$  and  $s_0(t)$  given by (4.8b). Then the time-dependent bound*

$$f(x, t) = s_{\max}(t) - \sigma(t)$$

can be estimated from below by the inequality

$$f(x, t) \geq f(x) \exp \left( \int_0^t s_{\max}(t')^3 dt' \right) \quad \forall x \in U(t). \tag{4.17}$$

*Proof* We estimate the time derivative of  $\sigma$  by a series of steps:

$$\begin{aligned} \partial_t s_{\max}(t) - \partial_t f(x, t) &= (s_{\max} - f)^2 \left( (s_{\max} - f)^2 - s_0^2 \right) \\ &\stackrel{x \in P}{\leq} s_{\max}^2 \left( s_{\max}^2 - s_0^2 - 2\tilde{f}s_{\max} + f^2 \right) \\ &\stackrel{f \leq s_{\max}}{\leq} \partial_t s_{\max} - f s_{\max}^3. \end{aligned}$$

Now one can subtract  $\partial_t s_{\max}(t)$  and the assertion follows after using Gronwall’s lemma for  $f(x, t)$ . In the last step we used  $f(x, t) \leq s_{\max}(t)$ , which follows again from positivity of  $\sigma$  in (4.16). When we simplified the ordinary differential equation and found an explicit expression for  $f(x, t)$ , we also reduced the size of the set where the bound is valid. At time  $t$  the inequality holds in  $U(t) = U \cup P(t)$ . □

But as we will see, this rough estimate suffices to show blow-up of  $s$  in finite time for a huge class of initial data. The following lemma provides the lower bound  $\tilde{p}(t) < p(t)$  that we need in order to prove the finite-time blow-up of  $s$ .

**Lemma 4.4** *Let the initial data be such that  $s_{\max}(0) > s_0(0) > 1$ , then  $p(t)$  is bounded from below by*

$$p(t) \geq C_1 (t + C_2)^{-2} s_{\max}(t)^{-8}. \quad (4.18)$$

*Proof* Using  $M_\epsilon = \{x \in \Omega : \epsilon < s_i(x) < s_0(t) - \epsilon\}$  the time-derivative is bounded by  $\partial_t s \geq -s_0^2 s^2 \geq -s_{\max}^2 s^2$ , which in turn implies

$$s(x, t) \geq \frac{1}{\epsilon^{-1} + t s_{\max}^2} \geq c_1 s_{\max}^{-2} (t + c_2)^{-1} \quad (t \geq 0, \forall x \in M_\epsilon), \quad (4.19)$$

where it was used that  $\int_0^t s_{\max}(s) ds < t s_{\max}(t)$ . Note that the size of the set  $m(t) = |M_\epsilon|$  is an increasing function. Then we use the integro-differential equation to bound  $p(t)$  as follows

$$\begin{aligned} p(t) s_{\max}^4 &\geq p(t) \partial_t s_{\max} \geq \int_P \partial_t s \, dx \\ &= - \int_N \partial_t s \, dx \geq - \int_{M_\epsilon} \partial_t s \, dx \\ &\geq \int_{M_\epsilon} s^2 (s_0^2 - (s_0 - \epsilon)^2) \, dx \geq c_3 \int_{M_\epsilon} s^2 \\ &\geq m(0) c_3 \min_{M_\epsilon} s^2 \stackrel{(4.19)}{\geq} C_1 s_{\max}^{-4} (t + C_2)^{-2} \end{aligned}$$

which was to be shown.  $\square$

In the next lemma we combine both lemmas to show blow-up of  $s$ . It remains an open question, to which extent this proof can be extended if the maximum is unique but the solution is not bounded by such a power law, e.g.,  $s_i(x) = \alpha_n (e^{-1/x^n} - e^{-1})$  initial data ( $\alpha_n$  is the normalization factor). For sufficiently large  $n$  the estimates in our proof do not suffice to show blow-up of  $s$  in a finite time.

**Theorem 4.5** *Let  $s(x, t)$  be a solution of (4.8) with non-negative, decreasing initial data  $s_i(x)$ . Suppose, in a small neighborhood of  $x = 0$  we have an upper bound*

$$s_i(x) \leq s_{\max}(0) - Cx^n$$

*for some arbitrary  $C, n > 0$ . Then  $s_{\max}(t)$  blows up after a finite time.*

*Proof* First of all, volume conservation implies

$$p(t) s_0(t) \leq 1. \quad (4.20)$$

In Theorem 4.2 we showed that  $s_{\max}(t)$  is unbounded. Suppose  $s_0(t)$  is bounded, then the integro-differential equation immediately implies blow-up of  $s$  after a finite time. Suppose  $s_0$  is unbounded, then (4.20) reveals that  $P(t) \subset U$  holds after a finite time. Presume that this is already true initially at  $t = 0$  and apply (4.17) from Lemma 4.3 with time-dependent  $x = p(t)$ . The upper bound  $s_i(x) < s_{\max}(0) - Cx^n$  implies  $s_{\max} > s_0 > 1$  which makes the application of (4.18) from Lemma 4.18 possible. Thus we obtain the inequality

$$\begin{aligned} s_{\max}(t) &\geq s_{\max}(t) - s(p(t), t) \geq f(t, p(t)) \\ &\geq f(p(t)) \exp \left( \int_0^t s_{\max}(t')^3 \, dt' \right) \\ &\geq f \left( C_1 s_{\max}^{-8} (t + C_2)^{-2} \right) \exp \left( \int_0^t s_{\max}(t')^3 \, dt' \right) \\ &= C C_1^n s_{\max}^{-8n} (t + C_2)^{-2n} \exp \left( \int_0^t s_{\max}(t')^3 \, dt' \right). \end{aligned}$$

In order to rewrite this inequality in terms of a differential inequality, which is easier to deal with, define  $q(t) = \int_0^t s_{\max}(t')^3 dt'$  and insert it into the previous estimate. This yields the differential inequality

$$(\partial_t q)^{\frac{8n+1}{3}} \geq CC_1^n (t + C_2)^{-2n} \exp(q) \quad \text{for } t \geq 0,$$

with  $q(0) = 0$ . We end up with the following convenient expression after rescaling  $t$  and  $q$  with a finite but  $n$  dependent scale

$$\partial_t q \geq (t + c)^{-\alpha} \exp(q) \tag{4.21}$$

with  $\alpha = \frac{6n}{8n+1} < 1$ . By explicit integration we get

$$q(t) \geq -\log \left( 1 - \frac{(t + c)^{1-\alpha} - c^{1-\alpha}}{1 - \alpha} \right), \tag{4.22}$$

which has a blow-up after a finite time. □

The estimates that are used in this proof are quite rough. Therefore we check the leading-order singular behavior of our estimate and compare with the expectation  $h(x_*, t) \sim (t_* - t)^{1/3}$ . Differentiating the lower bound

$$q(t) = -\log \left( 1 - \frac{(t + c)^{1-\alpha} - c^{1-\alpha}}{1 - \alpha} \right) = -\log(w(t)),$$

with respect to time gives

$$s_{\max}(t)^3 = \partial_t q(t) \sim \frac{w'(0)}{t_{**} - t} + O(1),$$

which has the expected behavior<sup>2</sup> and justifies our rough estimates.

#### 4.5 Finite-time pinch-off for a very viscous jet

As it was mentioned earlier, basic ideas and notion of the previous proof are lend from the paper by Renardy on jet pinch-off in finite time [14]. In his proof Renardy assumed differentiability of the initial data and used an essential auxiliary lemma, which unfortunately turned out to be incorrect (and also the corrigendum in [14]).

We use (4.17) to estimate the upper bound. This approach different because it makes no use of the property used in Renardy’s auxiliary lemma, and it’s more general because no differentiability of initial data is required.

The same technique can be applied to the jet pinch-off model very easily, because the model differs only slightly from (4.8). Consider the following equations describing inertialess pinching of a liquid thread [10, 14]

$$\partial_t s(x, t) = s(x, t)^{3/2} \left( \sqrt{\frac{s(x, t)}{s_0(t)}} - 1 \right), \tag{4.23a}$$

$$s_0^{1/2}(t) = \int_{\Omega} s(x, t)^2 dx \Big/ \int_{\Omega} s(x, t)^{3/2} dx. \tag{4.23b}$$

The initial data are non-negative, decreasing and normalized as in (4.9).

All properties of Lemma 4.1 can be carried over to (4.23). The computation of  $\partial_t s_0 > 0$  can be found in [14]. For jet pinch-off we compare solutions with solutions of the auxiliary ordinary differential equation

$$\partial_t \sigma = \sigma^{3/2} \left( \frac{\sigma^{1/2}}{s_0^{1/2}} - 1 \right), \tag{4.24}$$

and obtain the following lemma.

<sup>2</sup> Note that  $t_{**}$  denotes the zero of  $w(t)$ .



**Lemma 4.6** Let  $\sigma(x, t)$  be a solution of (4.24) and define  $f(x, t) = s_{\max}(t) - \sigma(x, t)$  for every  $x \in U$ . Then the following estimate holds:

$$f(x, t) \geq f(x) \exp\left(\frac{1}{2} \int_0^t s_{\max}(t')^{1/2} dt'\right), \quad \forall x \in U \cap P(t). \quad (4.25)$$

Note that  $P(t)$  is shrinking.

*Proof* With the previous definition of  $\sigma$  and  $f$  the following steps are obvious:

$$\begin{aligned} \partial_t s_{\max}(t) - \partial_t f(x, t) &= \partial_t \sigma = (s_{\max} - f)^{3/2} \left[ \left( \frac{s_{\max} - f}{s_0} \right)^{1/2} - 1 \right] \\ &\stackrel{x \in P}{\leq} s_{\max}^{3/2} \left[ \left( \frac{s_{\max} - f}{s_0} \right)^{1/2} - 1 \right] \\ &\leq s_{\max}^{3/2} \left[ \left( \frac{s_{\max}}{s_0} \right)^{1/2} \left( 1 - \frac{f}{2s_{\max}} \right) - 1 \right] \\ &= \partial_t s_{\max} - \frac{f}{2} \frac{s_{\max}}{s_0^{1/2}}. \end{aligned}$$

The assertion follows again after applying Gronwall's lemma to the differential inequality and using the initial data  $f(0, x) = f(x)$ .  $\square$

Similar to the previous theorem we need a lower bound to the size of  $p(t)$ .

**Lemma 4.7** If  $s_{\max}(0) > s_0(0) > 1$ , then  $p$  is bounded by

$$p(t) \geq C_1 s_{\max}^{-2} (t + C_2)^{-3} \quad \text{for } t \geq 0 \quad (4.26)$$

*Proof* Analogous to proof of (4.18).  $\square$

**Theorem 4.8** Let  $s(x, t)$  be a solution of (4.23) with non-negative, decreasing initial data  $s_i(x)$ . In an neighborhood of  $x = 0$  we have

$$s_i(x) \leq s_{\max}(0) - Cx^n$$

for some  $C, n > 0$ . Then  $s_{\max}(t)$  blows up after a finite time.

*Proof* Like in the proof for rupture in finite time we find

$$\begin{aligned} s_{\max}(t) &\geq f(x, t) \geq C (p(t))^n \exp\left(\frac{1}{2} \int_0^t s_{\max}(t')^{1/2} dt'\right) \\ &\geq C C_1^n s_{\max}^{-2n} (t + C_2)^{-3n} \exp\left(\frac{1}{2} \int_0^t s_{\max}(t')^{1/2} dt'\right). \end{aligned}$$

and define  $q(t) = \int_0^t s_{\max}(t')^{1/2} dt'$ . After rescaling  $q$  and  $t$  we obtain the differential inequality  $\partial_t q \geq (t + c)^{-(3n)/(4n+2)} \exp(q)$  which implies pinch-off after a finite time.  $\square$

Analogous to the previous proof we find that the estimate reproduces the known leading order singular behavior  $s_{\max}(t) \simeq C(t_{**} - t)^{-2}$  [8, 10].

## 5 Conclusions and outlook

We have studied the evolution of the rupture process for a dewetting film with large effective slip at the liquid–solid interface. We identified three different regimes, each with its own dominant balances and similarity solutions with different exponents. For regime II, we have a similarity solution of the second kind. By solving a boundary-value problem for a nonlinear ODE system, we have determined the similarity exponents; in fact, we obtained a discrete set of exponents for which an analytic similarity profile exists and is suggested to be unique. A formal proof will be given in the upcoming work described further below. Of this discrete family of solutions, only the “lowest order” is consistent with the terms neglected in the dominant balance considered in regime II.

Another important question in this paper was to prove that the solution  $s$  in regime II blows up after a finite time. This depends very much on the local behavior of the initial data near the maximum. If the maximum is attained in a finite interval, then the solution stays bounded. In all other cases solutions are unbounded. For initial data are that bounded from above, like

$$s_i(x) \leq s_{\max}(0) - Cx^n,$$

for some  $C, n > 0$ , we proved that blow-up occurs after a finite time. In the proof we obtained a lower bound on the blow-up rate which reproduces the known rate for jet pinch-off and the rate  $h(x_*, t) \sim (t_* - t)^{1/3}$  for thin-film rupture that we found in the third section.

Slight changes of the initial data near the maximum of  $s_i(x)$  can change the later behavior qualitatively. In the theory of Ostwald ripening self-similar solutions show a similar sensitive dependence on the initial data; this dependence is associated with the term *weak selection* [28,29]. In an upcoming paper [30,31] we will explain how the local behavior of the initial data influences the emerging self-similar solutions for second-kind similarity solutions of (4.8).

**Acknowledgments** Andreas Münch acknowledges support by a Heisenberg Scholarship DFG-grant MU 1626/3-2. Dirk Peschka was supported by a graduate student scholarship within the DFG research training school 1128. The authors would like to thank Barbara Wagner for helpful discussions.

## References

1. Constantin P, Dupont TF, Goldstein RE, Kadanoff LP, Shelley MJ, Zhou S-M (1993) Droplet breakup in a model of the Hele-Shaw cell. *Phys Rev E* 47:4169–4181
2. Zhang WW, Lister JR (1999) Similarity solutions for van der Waals rupture of a thin film on a solid substrate. *Phys Fluids* 11: 2454–2462
3. Erneux T, Davis SH (1993) Nonlinear rupture of free films. *Phys Fluids A* 5:1117–1122
4. Ida MP, Miksis MJ (1996) Thin film rupture. *Appl Math Lett* 9:35–40
5. Bertozzi AL, Brenner MP, Dupont TF, Kadanoff LP (1994) Singularities and similarities in interface flows. In: L. Sirovich (ed) *Trends and perspectives in applied mathematics*. *Appl Math Sci* 100:155–208. Springer, New York
6. Vaynblat D, Lister JR, Witelski TP (2001) Symmetry and self-similarity in rupture and pinchoff: a geometric bifurcation. *Eur J Appl Math* 12:209–232
7. Oron A, Davis SH, Bankoff SG (1997) Long-scale evolution of thin liquid films. *Rev Mod Phys* 69:931–980
8. Eggers J (1997) Nonlinear dynamics and breakup of free-surface flows. *Rev Mod Phys* 69:865–930
9. Eggers J (1993) Universal pinching of 3D axisymmetric free-surface flow. *Phys Rev Lett* 71:3458–3460
10. Papageorgiou DT (1995) On the breakup of viscous liquid threads. *Phys Fluids* 7:1529–1544
11. Brenner MP, Lister JR, Stone HA (1996) Pinching threads, singularities and the number 0.0304... *Phys Fluids* 8:2827–2836
12. Witelski TP, Bernoff AJ (1999) Stability of self-similar solutions for van der Waals driven thin film rupture. *Phys Fluids* 11: 2443–2445
13. Witelski TP, Bernoff AJ (2000) Dynamics of three-dimensional thin film rupture. *Physica D* 147:155–176
14. Renardy M (2001) Finite time breakup of viscous filaments *Z Angew Math Phys* 52:881–887; (2007) Corrigendum for “Finite time breakup of viscous filaments. *Z Angew Math Phys* 58:904–905
15. Becker J, Grün G, Seemann R, Mantz H, Jacobs K, Mecke KR, Blossey R (2003) Complex dewetting scenarios captured by thin film models. *Nat Mater* 2:59–63
16. Reiter G (1992) Dewetting of thin polymer films. *Phys Rev Lett* 68:75–78

17. Redon C, Brzoska JB, Brochard-Wyart F (1994) Dewetting and slippage of microscopic polymer films. *Macromolecules* 27: 468–471
18. Reiter G, Sharma A (2001) Auto-optimization of dewetting rates by rim instabilities in slipping polymer films. *Phys Rev Lett* 80:166103
19. Fetzer R, Jacobs K, Münch A, Wagner B, Witelski TP (2005) New slip regimes and the shape of dewetting thin liquid films. *Phys Rev Lett* 95:127801
20. Kargupta K, Sharma A, Khanna R (2004) Instability, dynamics and morphology of thin slipping films. *Langmuir* 20:244–253
21. Münch A, Wagner B, Witelski TP (2005) Lubrication models with small to large slip lengths. *J Eng Math* 53:359–383
22. Münch A (2005) Dewetting rates of thin liquid films. *J Phys Condens Matter* 17:S309–S318
23. Münch A, Wagner B (2005) Contact-line instability of dewetting thin films. *Physica D* 209:178–190
24. Kitavtsev G, Wagner B, Recke L (2008) Coarsening dynamics of slipping droplets. *J Eng Math*. doi:[10.1007/s10665-009-9313-z](https://doi.org/10.1007/s10665-009-9313-z)
25. Lauga E, Brenner MP, Stone HA (2007) Microfluidics: the no-slip boundary condition. In: Tropea C, Yarin A, Foss JF (eds) *Handbook of experimental fluid dynamics* Springer, Chapter 19, pp 1219–1240
26. Vaynblat D, Lister JR, Witelski TP (2001) Rupture of thin viscous films by van der Waals forces: evolution and self-similarity. *Phys Fluids* 13:1130–1140
27. Barenblatt GI (1996) Scaling, self-similarity, and intermediate asymptotics, volume 14 of Cambridge texts in applied mathematics. Cambridge University Press, Cambridge
28. Giron B, Meerson B, Sasorov PV (1998) Weak selection and stability of localized distributions in Ostwald ripening. *Phys Rev E* 58:4213–4216
29. Niethammer B, Pego RL (1999) Non-self-similar behavior in the LSW theory of Ostwald ripening. *J Stat Phys* 95:867–902
30. Peschka D, Niethammer B, Münch A (2008) Self-similar rupture of viscous thin films in the strong-slip regime. *Nonlinearity* (to appear)
31. Peschka D (2008) Self-similar rupture of thin liquid films with slippage. PhD Thesis, Institute for Mathematics, Humboldt University Berlin